Title: ER-localisation and activity of maize auxin biosynthetic enzymes

Verena Kriechbaumer[1*], Hyesu Seo[2], Woong June Park[2], Chris Hawes[1]

[1] Biological and Medical Sciences, Oxford Brookes University, Oxford OX3 0BP, UK

[2] Department of Molecular Biology, Institute of Nanosensor and Biotechnology, Dankook University, Yongin-si 448-701, South Korea

[*]**Correspondence**: Verena Kriechbaumer, vkriechbaumer@brookes.ac.uk

Plant Cell Biology, Biological and Medical Sciences, Oxford Brookes University, Oxford OX3 0BP, UK

Phone +44 (0)1865 483639

Fax: 44 (0)1865 483955

Email adresses:

vkriechbaumer@brookes.ac.uk, mohot@hanmail.net, parkwj@dku.edu, chawes@brookes.ac.uk.

Running title: auxin biosynthesis and the endoplasmic reticulum

Keywords: auxin biosynthesis, YUCCA, maize, *Zea mays*, localisation, compartmentation, endoplasmic reticulum.

Word count total: 7700

Word count Summary: 204

Word count Introduction: 790

Word count Results: 1586

Word count Discussion: 1949

28 Word count Experimental procedures: 1149

29 Word count References: 1697

30 Word count Figure legends: 512

31

32 We show that maize microsomes are capable of producing auxin and that two maize
33 auxin biosynthetic proteins -*Zm*SPI1 and *Zm*TAR1- are ER-localised therefore linking
34 auxin biosynthetic activity to the ER.

35

Summary

Auxin is a major growth hormone in plants and the first plant hormone to be discovered and studied. Active research over more than sixty years has shed light on many of the molecular mechanisms of its action including transport, perception, signal transduction and a variety of biosynthetic pathways in various species, tissues and developmental stages.

The complexity and redundancy of the auxin biosynthetic network and enzymes involved raises the question how such a system, producing such a potent agent as auxin, can be appropriately controlled at all.

Here we show that maize auxin biosynthesis takes place in microsomal as well as cytosolic cellular fractions from maize seedlings. Most interestingly, a set of enzymes shown to be involved in auxin biosynthesis via their activity and/or mutant phenotypes and catalysing adjacent steps in YUCCA-dependent biosynthesis are localised to the endoplasmic reticulum (ER). Positioning of auxin biosynthetic enzymes at the endoplasmic reticulum could be necessary to bring auxin biosynthesis in closer proximity to ER-localised factors for transport, conjugation and signalling and allow for an additional level of regulation by subcellular compartmentation of auxin action. Furthermore it might provide a link to ethylene action and be a factor in hormonal crosstalk as all five ethylene receptors are ER-localised.

Introduction

Auxin was the first major plant hormone to be discovered. Already Darwin proposed the existence of moving growth regulators (Darwin and Darwin, 1880). Kögl *et al* showed that auxin was present in plants and identified it as indole-3-acetic acid (Kögl *et al*., 1934). As the major plant growth hormone auxin is responsible for processes such as fruit ripening, photo- and gravitropism, and senescence, it has various applications in

63 agriculture and horticulture such as the stimulation of root growth in cuttings and
64 promotion of fruit production.
65 Biosynthesis of auxin is especially complex due to the existence of multiple pathways.
66 Depending on the organ, developmental stage or environment (Normanly and Bartel,
67 1999; Östin *et al*., 1999), parallel tryptophan-dependent and -independent pathways
68 (Woodward and Bartel, 2005; Kriechbaumer *et al*., 2006) may be differentially
69 regulated, creating a metabolic network that changes dynamically to maintain
70 homeostasis or supply IAA for local demands. Therefore finding a dominant
71 biosynthetic pathway has proved rather difficult and integrating data from the variety of
72 species studied in this respect is problematical (reviewed in Tivendale *et al*., 2014).
73
74 **YUCCA route in auxin biosynthesis**
75 Recent research especially focussed on the YUCCA route of auxin biosynthesis as
76 knockout of *YUCCA* genes in *Arabidopsis* resulted in the first ever reported auxin
77 depletion phenotype. YUCCA proteins are a family of flavin-dependent
78 monooxygenases that catalyse the conversion of indole-3-pyruvic acid (IPA) to the
79 auxin IAA (Mashiguchi *et al*., 2011; Kriechbaumer *et al*., 2012; Dai *et al*., 2013).
80
81 Previous research has shown that one of the *Arabidopsis YUCCA* genes (*YUCCA4*)
82 exists in two major splice isoforms. YUCCA4.2 features a C-terminal hydrophobic
83 transmembrane domain (TMD). This TMD was shown to be inserted into the ER
84 membrane with the remainder of the protein facing the cytosol (Kriechbaumer *et al*.,
85 2012).
86
87 **Subcellular localisation of auxin biosynthesis in maize**
88 Due to the intriguing subcellular localisation differences of YUCCA4 and potentially
89 other YUCCA proteins in *Arabidopsis* (YUCCA6, Kim *et al*., 2007; YUCCA3, 5, 10, 11 *in*

silico prediction, Kriechbaumer *et al*., 2012), it is of interest to know if such subcellular distribution of auxin biosynthesis is also present in economically important plants such as maize (*Zea mays*). In contrast to the 11 *YUCCA* genes in *Arabidopsis* only two main YUCCA candidates are described in maize: sparse inflorescence1 (*Zm*SPI1, Gallavotti *et al*., 2008) and *Zm*YUC1 (LeClere *et al*., 2010). *Zm*YUC2 and *Zm*YUC3 have high similarity to *Zm*YUC1 and *Arabidopsis* YUCCA proteins but extremely low transcript levels (Bernardi *et al*., 2012). Whereas in *Arabidopsis* multiple YUCCA genes have to be knocked out to produce a phenotype, in maize a single YUCCA knockout causes strong phenotypic effects. The mutant *spi1* shows severe developmental defects in the initiation of axillary meristems and lateral organs during vegetative and inflorescence development (Gallavotti *et al*., 2008). Especially interesting here is that even in a quadruple *Arabidopsis yucca* mutant the IAA levels are still 50% of WT levels (Stepanova *et al*., 2011) whereas the maize mutant *defective endosperm 18 (de18)*, containing a mutation in *Zm*YUC1, only contains around 5% of WT IAA levels in the endosperm (Bernardi *et al*., 2012). The mutant endosperm also displays a lower cell number, smaller cells and impaired endoreduplication. It was therefore concluded that *Zm*YUC1 is crucial for normal endosperm development in maize. The *spi1* mutation in a *YUC* ortholog is the result of a point mutation in the FAD-binding domain (Gallavotti *et al*., 2008). This mutation shows auxin deficiency phenotypes but mutant plants still have more than 80% of normal free IAA (Phillips *et al*., 2011).

The enzymatic step before YUCCA, the conversion of tryptophan to IPA, is catalysed by tryptophan aminotransferases. The tryptophan aminotransferase of *Arabidopsis* (TAA1) was shown to be responsible for rapid changes in IAA levels in shade avoidance (Stepanova *et al*., 2008; Tao *et al*., 2008). *taa1* mutants display reduced auxin levels (Tao *et al*., 2008). *Zm*TAR1 (Chourey *et al*., 2010), *Zm*VT2 (Phillips *et al*., 2011) and *Zm*TAR3 (*Zm*Alliin1, Bernardi *et al*., 2012) are named as TAA1 orthologs in

maize. *vt2* mutants are severely impaired in vegetative and reproductive development in height and inflorescence and show reduced free IAA levels (Phillips *et al*., 2011). A double mutant of *vt2* and *spi1* had the same IAA reduction as a *vt2* or *spi1* single mutant indicating that *Zm*VT2 and *Zm*SPI1 act in the same pathway (Phillips *et al*., 2011).

Here we report on the finding that auxin biosynthetic activity using either tryptophan (Trp) or indole-3-pyruvic acid (IPA) as substrates can be found in the microsomal fraction of maize roots and coleoptiles. In accordance with that we show that at least three of maize auxin biosynthetic proteins are localised to ER membranes. This points towards a model of auxin function that involves ER-membrane localisation and subcellular compartmentation as an additional level of regulation.

Results

Bioinformatics analysis of enzymes in the maize YUCCA pathway

In silico analysis of enzymes suggested to be involved in the YUCCA route of maize auxin biosynthesis predicted a potential N-terminal hydrophobic transmembrane domain (TMD) for *Zm*SPI1 and *Zm*TAR1 (Figure 1, Table 1). According to the algorithm TMHMM *Zm*SPI1 features an N-terminal TMD between the amino acid (aa) 20 and 42 for membrane insertion with the C-terminus facing the cytosol. For *Zm*TAR1 the program predicts an N-terminal TMD between aa 13 and 35 with the C-terminal rest of the protein facing the cytosol (Figure 1, Table 1). Because N-terminal transmembrane helices could easily act as signal peptides, the algorithm SignalP4.1 was applied but predicted no signal peptides for *Zm*SPI1 or *Zm*TAR1 (Table 1).

142 *Zm*TAR3 features a hydrophobic N-terminal sequence with a strongly predicted signal
143 peptide for transfer into the ER. According to SignalP4.1 a potential signal peptide
144 cleavage could occur after aa 24 (Table 1).
145 Another set of proteins in the YUCCA pathway of auxin biosynthesis (*Zm*YUC1 and
146 *Zm*VT2) are predicted to be cytosolic and do not feature any hydrophobic domains.
147 TMHMM indicates weak TMDs for these proteins but their probability calculations put
148 them far below the cut-off threshold (Figure 1).
149
150 **Auxin biosynthetic activity in maize microsomes**
151 To test for auxin biosynthesis in or on microsomes a protocol to isolate active ER-
152 microsome fractions from maize coleoptiles (Col) and primary roots (PR) was carried
153 out (adapted from soybean extraction, Abell *et al*., 1997).
154 To determine the purity of the microsomal fraction a Western blot of both the
155 microsomal and cytosolic fraction with antibodies raised against the cytosolic maize
156 nitrilase 1 protein (*Zm*NIT1) was performed (Figure 2A). This antibody was shown to
157 easily detect nitrilase 1 and 2 protein in various tissues in the range of ng/mg total
158 protein (Park *et al*., 2003; Kriechbaumer *et al.,* 2007). The microsomal fraction showed
159 no detectable nitrilase protein. Furthermore to account for potential plasma membrane
160 contamination the microsomal fraction and total protein extract were blotted with anti-
161 H+ATPase antibodies. This antibody recognises the plasma membrane protein
162 H+ATPase in a variety of plants and fungi including *Zea mays* and *Arabidopsis*. A
163 corresponding band could be detected in total protein extract but not in the microsomal
164 fraction (Figure 2B). Contamination of the microsomal fraction with mitochondria was
165 tested using anti-AOX1/2 antibodies. The alternative oxidases (AOX) are quinol
166 oxidases located in the plant inner mitochondrial membrane. This mitochondrial marker
167 protein could be detected in the total protein extract but not in the microsomal fraction
168 (Figure 2B).

Enzymatic activity tests were performed with the microsome fractions, the cytosolic supernatant and total extract from maize coleoptiles or primary roots four days after germination. Respectively, the precursor tryptophan (Trp) and the intermediate in the YUCCA pathway (Figure 1) indole-3-pyruvic acid (IPA) were used as substrates. Assays in 100 mM Tris-HCl, pH 8.0, consisted of 20 µl plant extract, 1 mM NADPH, 100 µM FAD and 100 µM Trp or IPA in a total volume of 100 µl, were incubated for 1 h in a 37ºC water bath. Controls with boiled protein were included and unspecific IAA conversion was deducted from the assays. After the incubation the assays were snap-frozen in liquid nitrogen and IAA was extracted by ethyl acetate phase separation. IAA was quantified via HPLC in isocratic flow of 0.8 ml/min with a 40:60 mixture of buffer A (10% methanol, 0.3% acetate) and buffer B (90% methanol, 0.3% acetate).

Auxin biosynthetic activity with Trp and IPA was found in microsomal as well as cytosolic fractions of maize coleoptiles and primary roots (Figure 3). The microsome fraction of the coleoptiles shows nearly half the activity with tryptophan as well as IPA compared to the corresponding cytosolic fraction (Figure 3A). In primary root tissue the Trp conversion in the microsomal fraction is nearly a quarter of the cytosolic activity and IPA turnover nearly double the Trp conversion (Figure 3B). To validate these results gas chromatography–mass spectrometry (GC-MS) was performed using 2,4,5,6,7-pentadeuteriated IAA (Cambridge Isotope Laboratories, UK) as internal standard to account for losses in IAA during protein preparation and IAA purification (Figure S1 and S2). The samples were derivatized using ethereal diazomethane and the identity of derivatized IAA was confirmed by 130 and 189 fragmentation ions and normalized against the internal standard recognized by 135 and 184 fragmentation ions. Representative examples of GC-MS data traces for the conversion of Trp and IPA, respectively, to IAA in microsomal and cytosolic fractions are shown in Figure S1.

196 Boiled controls for the enzymatic conversion data shown are included (Figure S1). The
197 internal standard used in the mass spectrometry analysis allows accounting for loss of
198 IAA molecules during sample preparation. A comparison between GC-MS and HPLC
199 data shows that approximately 50% of IAA could be lost during the analysis steps
200 (Figure S2A) but the ratio between activity in the microsomal fractions compared to the
201 cytosolic fractions are highly similar (Figure S2B).
202 In summary his enzymatic data indicates that tryptophan-dependent auxin biosynthesis
203 partly takes part on or in the endoplasmic reticulum (being the major component of
204 microsomal fractions) and, as IPA is converted even to a higher extent, very likely via
205 the YUCCA pathway.
206
207 **Subcellular localisation of auxin biosynthetic enzymes**
208 As auxin activity could be detected in both the cytosol and ER fractions one could
209 predict the presence of auxin-producing enzymes in or on both compartments.
210 Furthermore, as activity with the substrates Trp and IPA could be found in microsomes
211 both a tryptophan aminotransferase as well as a YUCCA homologue should be
212 present. Proteins of interest in this respect were, of course, enzymes with predicted TM
213 domains and therefore with a potential ER membrane localisation. *Zm*TAR1 and
214 *Zm*SPI1 feature TM domains with high probability, *Zm*YUC1 shows potential for a TMD
215 but below the prediction cut-off (Table 1).
216 Proteins of interest were fused to C-terminal YFP fluorescent tags, respectively, so as
217 not to interfere with the predicted N-terminal TMDs. These fusion proteins were co-
218 expressed transiently in tobacco leaves with the ER marker GFP-HDEL (Figure 4, lane
219 1-3) and visualised by confocal microscopy. As predicted by their domain structure both
220 *Zm*SPI1 and *Zm*TAR1 (Figure 4, lane 1 and 2) localise indeed to the ER, whereas
221 *Zm*YUC1 appears cytosolic (Figure 4, lane 3). Furthermore *Zm*YUC1 shows
222 colocalisation with the plasma membrane marker LTI6b-GFP (Martinière *et al*., 2012;

223 Figure 4, lane 4). As a very weak TMD below the positive prediction threshold was
224 predicted for *Zm*VT2 the N-terminal 200 aa of this protein were used for localisation
225 studies. In coexpression with GFP-HDEL it was shown that as predicted *Zm*VT2 stays
226 in the cytoplasm and does not localise to the ER (Figure 4, lane 5). However, the N-
227 terminus of *Zm*TAR3 featuring an N-terminal TMD and signal peptide clearly labelled
228 the ER but also showed some larger bright punctae. To quantify the colocalisation of
229 the auxin constructs and the ER marker HDEL Pearson's correlation coefficients in the
230 colocalized volume (R_{coloc}) were determined using the ImageJ software. In this analysis
231 an R_{coloc} of 1 indicates a perfect correlation with the ER marker, a value of 0 shows no
232 correlation. As to be expected the ER-membrane proteins *Zm*SPI1, *Zm*TAR1 and
233 *Zm*TAR3 showed with an R_{coloc} of 0.4775, 0.6819 and 0.5837, respectively, far higher
234 colocalisation coefficients than the cytosolic proteins *Zm*YUC1 and *Zm*VT2 with an
235 R_{coloc} of 0.0769 and 0.0438, respectively.
236
237 **ER-Membrane topology of *Zm*SPI1 and *Zm*TAR1**
238 To determine if the C-terminal enzymatic domains of *Zm*SPI1 and *Zm*TAR1 are
239 residing in the ER lumen or the cytosol, a redox-sensitive fluorescent tag (roGFP2,
240 Brach *et al*., 2009) was fused to the C-termini of both proteins. This special GFP form
241 allows ratiometric quantification of the redox potential as disulphide bonds are formed
242 between surface-exposed cysteine residues. This affects the ratio of excitation by
243 wavelengths of 405 or 488 nm. For analysis the Matlab program Batch Ratio Analysis
244 V1.3 (Dr M. Fricker, Oxford University; Schwarzländer *et al*., 2008) was used. A high
245 fluorescence ratio at 405/488 nm (Figure 5, pseudo-coloured in red) would point to the
246 protein facing the oxidizing environment of the ER lumen, whereas a low ratio (pseudo-
247 coloured in blue) indicates that it is located in the more reduced environment of the
248 cytosol. *Zm*SPI1-roGFP2 and *Zm*TAR1-roGFP2 have excitation ratios of 0.36 and 0.33
249 (Figure 5, lane 1 and 2), respectively. These ratios are closer to that of cytosolic

roGFP2 (0.17) (Figure 5, lane 3) than that of luminal roGFP2–HDEL (1.31) (Figure 5, lane 4), indicating that the C-termini of both *Zm*SPI1 and *Zm*TAR1 face the cytosol.

To show that the tagged enzymes are indeed functional *in planta* and capable to contribute to auxin biosynthesis, the ER-localised proteins *Zm*SPI1-YFP or *Zm*TAR1-YFP, respectively, were transiently expressed in tobacco leaf epidermal cells and auxin biosynthetic activity was quantified (Figure 6). To control for effects on auxin biosynthesis induced by the transformation event controls using an empty vector as well as a vector coding for the ER-marker GFP-HDEL were included. For these activity assays plant sections infiltrated with *Zm*SPI1 were tested with the enzyme's substrate IPA. Protein extracts from leaves infiltrated with *Zm*SPI1 resulted in a significant 47% increase in activity (Figure 6A). For leaves infiltrated with *Zm*TAR1 Trp was used as a substrate and this overexpression resulted in a 39% increase in microsomal auxin activity compared to empty vector and GFP-HDEL controls (Figure 6B). Furthermore free IAA was measured in leaves infiltrated with *Zm*SPI1, *Zm*TAR1 or *Zm*YUC1, respectively, and compared to an empty vector control (Figure 6C). Expression of each of the three constructs increased the free IAA content significantly by 18, 10 and 14%, respectively.

DISCUSSION

Local auxin action

Auxin controls developmental processes via gradients at the tissue level. These gradients are created by localised auxin biosynthesis as well as transport (Kramer and Bennett, 2006). To comprehend local auxin effects and gradient formation an understanding of where auxin biosynthesis occurs and how it is controlled is crucial.

276 The *Arabidopsis* YUCCA4.2 was the first auxin biosynthetic protein shown to have ER
277 localisation with a transmembrane domain anchoring the protein into the ER membrane
278 but its active enzymatic domain facing the cytosol (Kriechbaumer *et al*., 2012).
279 Furthermore YUCCA6 has been shown to be non-cytosolic (Kim *et al*., 2006) and
280 YUCCA3, 5, 10 and 11 feature TMDs or signal peptides (Kriechbaumer *et al*., 2012).
281 *Arabidopsis* TAA1 does not feature any TMDs and is predicted to be cytosolic. The
282 functional importance of this localisation remains so far unclear especially as this splice
283 version is only detectable in flower tissue, but connecting auxin biosynthesis with the
284 ER surface might allow closer proximity and therefore auxin transport into the ER for
285 example for storage or an additional level of regulation.
286
287 Maize has proven to be a useful tool for researching potential subcellular
288 compartmentation. Other than *Arabidopsis* with 11 *YUCCA* genes, in maize, only
289 sparse inflorescence1 (*Zm*SPI1, Gallavotti *et al*., 2008) and *Zm*YUC1 (LeClere *et al*.,
290 2010) are described as its main auxin producing enzymes; both producing strong
291 phenotypes *in planta* showing their significance and contribution. Despite strong auxin
292 phenotypes, IAA levels are hardly changed in *Arabidopsis YUC* overexpression
293 (Stepanova *et al*., 2011) which raises the question as to whether the effects are due to
294 other yet unidentified compounds or if accumulation is localised to certain tissues
295 (Tivendale *et al*., 2014). Another influential factor could be the subcellular localisation
296 and membrane anchoring of auxin biosynthetic enzymes.
297 Auxin biosynthetic activity could be detected in microsomal fractions of both root and
298 coleoptile tissue of young maize seedlings. It was shown that the “whole” biosynthetic
299 pathway from Trp to IAA as well as the last step in the YUCCA pathway, IPA to IAA,
300 takes place (Figure 3). The fact that both conversions are present is especially
301 important as it has been previously reported that IPA easily degrades to IAA at room
302 temperature (Koga *et al*., 1992). In this study it was observed that IPA is absolutely

303 unstable when dissolved in water but has to be made up freshly before each
304 experiment and dissolved in ethanol or methanol. Interestingly when then mixed in with
305 the boiled-control plant extracts IPA is stable with less than 5% unspecific conversion to
306 IAA. After detecting the presence of YUCCA-dependent auxin biosynthetic activity in
307 these microsomal fractions, the question about the corresponding enzymes linked to
308 the ER compartment has been raised. Prediction algorithms pointed at *Zm*TAR1 and
309 *Zm*SPI1 as potential candidates that have shown auxin activity and phenotypes
310 (Gallavotti *et al*., 2008; Chourey *et al*., 2010) as well as potential TMDs capable of
311 anchoring them to the ER (Figure1, Table 1). Both *Zm*TAR1 and *Zm*SPI1 were indeed
312 shown to localise to the ER (Figure 4). Additionally *Zm*TAR3 which has only recently
313 been described as a TAA1 homologue (Bernardi *et al*., 2012), features an N-terminal
314 hydrophobic sequence including a signal peptide (Table 1) and also displays ER
315 localisation. Both *Zm*TAR1 and *Zm*TAR3 are simultaneously expressed in developing
316 endosperm coinciding with highest IAA levels at this specific developmental stage
317 (LeClere *et al*., 2008; Bernardi *et al*., 2012). It was suggested that this is an indication
318 of redundancy or that the resulting IPA is used for different pathways (Bernardi *et al*.,
319 2012); with *Zm*TAR1 facing the cytosol and *Zm*TAR3 predicted to cross the ER
320 membrane due to its signal peptide this could indicate interesting aspects for fine-
321 tuning or indeed the use of IPA in two different pools.
322
323 The ER localisation of maize proteins involved in auxin biosynthesis reported here as
324 well as the previously shown ER localisation of *Arabidopsis* YUCCA4.2 (Kriechbaumer
325 *et al*., 2012) indicates an additional level of subcellular compartmentation in auxin
326 biosynthesis. Auxin action might not only be reliant on auxin levels and free versus
327 conjugated auxin but furthermore its actual or relative concentration in different
328 subcellular compartments.
329

Localisation of other aspects of auxin biology: transport, signalling and conjugation

This ER localisation of auxin biosynthetic enzymes may well also be connected to other parts of auxin biology. A duality of localisation of proteins involved in auxin action other than its biosynthesis can be seen in auxin transport, signalling and conjugation (Figure 7).

Pinformed (PIN) auxin efflux carriers are localised at the plasma membrane (PIN1-4 and PIN7) and mediate directional cell-to-cell auxin transport whereas PIN5 (Mravec *et al*., 2009) and PIN8 (Dal Bosco *et al*., 2012) are ER localised. PIN5 is suggested to transport auxin from the cytosol into the ER (Mravec *et al*., 2009) but PIN5 gain of function also results in decreased free IAA and an increase in conjugated auxin. It was recently suggested that intercellular auxin transport is even regulated by PIN5-dependent auxin transport between the ER and the cytoplasm (Wabnik *et al*., 2011).

Like PIN5 the PILS2 and PILS5, members of a recently discovered transporter family, increase auxin conjugation but decrease nuclear auxin signalling presumably by auxin transport in to the ER where it is inaccessible for nuclear signalling (Barbez *et al*., 2012). Furthermore PILS2 and PILS5 influence the ratio between free and conjugated IAA suggesting a role for these protein in regulating auxin metabolism (Barbez *et al*., 2012). Together, PIN5, PILS2 and PILS5 increase auxin compartmentation between the cytosol and the ER whereas the pollen specific PIN8 decreases compartmentation antagonistically.

Colocalisation and interaction studies between ER localised auxin biosynthetic enzymes and the transporters PIN5, PIN8, PILS2 and PILS5 would elucidate potential functional interfaces between auxin biosynthesis and signalling. With PIN5 and 8 and PILS2 and 5 altering the auxin conjugation rates and thereby linking transport to

metabolism, it could be speculated that auxin conjugation might happen in the ER (Barbez and Kleine-Vehn, 2013).

Of further interest in the potential of subcellular compartmentation and in understanding of the mechanism of such will therefore be the location of auxin conjugation and deconjugation. In *Arabidopsis* amidohydrolases have been shown to contribute free IAA to the auxin pool during germination (Rampey *et al*., 2004). In *Arabidopsis* ILR1-like amidohydrolases 3 (ILL3) has a strong prediction for a secretory signal peptide (TargetP possibility: 0.965), ILL2 features an ER retention signal (Bitto *et al*., 2009) and ILL1, ILL4 and ILL5 are predicted to contain a signal peptide and a C-terminal ER retrieval sequence (reviewed in Ludwig-Müller, 2011). The maize homologue has a very low and uncertain prediction for such (TargetP possibility: 0.262).

Its counterpart, the auxin conjugase GH3 is predicted to be cytosolic in both maize and *Arabidopsis* and has been shown to be localised in the cytosol in *Physcomitrella patiens* (Ludwig-Müller *et al*., 2009). Nonetheless, cytosolic activity of GH3 has not yet been shown and the possibility of ER localised GH3 proteins or other proteins with conjugating functions in higher plants cannot be excluded (Ludwig-Müller, 2011; Barbez and Kleine-Vehn, 2013). Further investigation of which enzymes exactly are involved into this process as well as their subcellular localisation and the location of auxin conjugation and deconjugation will be of invaluable interest.

It has to be mentioned though that during germination in the tissue used in this study the main source of free IAA is the hydrolysis of IAA-inositol-arabinose and IAA-inositol-galactose. These compounds accumulate in the kernel during kernel development via the formation of IAA-glucose, transesterification to IAA-inositol and further glycosylation to IAA-inositol-arabinose and IAA-inositol-galactose (Labarca *et al*., 1965; Ueda and Bandurski, 1974; Bandurski, 1980). In maize the enzyme responsible for the first step

383 in this conjugation is coded by the *iaglu* gene (Szerszen *et al*., 1994). TargetP
384 prediction for *iaglu* homologues in maize and Arabidopsis is inconclusive; the algorithm
385 PSORT predicts a cytosolic localisation with a certainty of 0.450.
386
387 **Functional protein complexes**
388 Metabolic functions of all higher organisms have to be strictly coordinated. Organellar
389 compartmentalization is an important mechanism for this on a cellular level. Most
390 cellular processes are carried out by interacting proteins assembled as multiprotein
391 complexes. Metabolons, functional multi-enzyme complexes held together by
392 noncovalent binding typically with stabilisation via membrane or cytoskeletal anchoring,
393 can add to this on a molecular scale. Metabolons allow substrate channelling, a direct
394 passing on of the product from an enzymatic reaction to act as substrate for the next
395 biosynthetic step. This increases substrate concentration and turnover rates, prevents
396 diffusion and metabolic interference, and is advantageous for instable or toxic
397 intermediates (reviewed in Møller, 2010). Such complex coordination has been shown
398 for protein translocases found in ER, chloroplasts and mitochondria (Jarvis *et al*., 1998;
399 Werhahn *et al*., 2001; Van den Berg *et al*., 2004). Here the C-terminal TMD operates as
400 assembly signal to form multimer complexes.
401 Metabolons have been shown for various enzymatic pathways in secondary
402 metabolism such as the synthesis of phenylpropanoids (Stafford, 1974) or flavonoids
403 (Hrazdina and Wagner, 1985; Winkel-Shirley, 2001). Enzymes producing cyanogenic
404 glucosides in sorghum have been found to form a metabolons in ER domains (Winkel,
405 2004). In the ER lipid micro-domains have been shown to allow for metabolons
406 assembly (Zajchowski and Robbins, 2002). Such rafts can even move metabolons
407 around in an actin-guided way if under pathogen attack (Chuong *et al*., 2004). It is a
408 possibility that metabolon formation allows production of the basic structures and
409 depending on developmental stage, tissue or stress situation additional enzymes could

410 be recruited to the metabolons for specific structural alterations or add regulatory
411 effects on the production line (Jørgensen *et al*., 2005).
412
413 **Conclusions**
414 All these findings reveal a formerly unanticipated way of regulating cellular
415 homeostasis of biosynthetic, signalling and transport compounds by their subcellular
416 compartmentalization.
417 In summary, we suggest a model where auxin biosynthesis via the YUCCA pathway is
418 not only purely cytosolic but also linked to the ER membrane (Figure 7). Interestingly
419 also auxin transporters of the PIN and PILS family and enzymes for hydrolysis of
420 conjugated IAA can be found on and in the ER. Furthermore various links between
421 auxin and ethylene signalling and biosynthesis have been described and with all five
422 ethylene receptors ER localised (Grefen *et al*., 2008) such close proximities could
423 potentially be important for hormonal crosstalk.
424
425 The question of a functional importance of such membrane anchoring of the
426 *Arabidopsis* YUCCA4.2 as well as the maize *Zm*SPI1 and *Zm*TAR1 remains open. So
427 far no phenotypes for *Arabidopsis yucca4* (neither the cytosolic form 4.1 nor the ER-
428 localised form 4.2) mutants or other single knockout mutants have been reported.
429 Maize *spi1* on the other hand is severely affected in vegetative and inflorescence
430 development (Gallavotti *et al*., 2008) despite mutant plants retaining more than 80% of
431 normal free IAA levels (Phillips *et al*., 2011). A loss of function in the cytosolic protein
432 *Zm*YUC1 results in impaired in endosperm development with reduction of mass and
433 free IAA as well as smaller cells at a lower number and compromised
434 endoreduplication in this tissue (Bernardi *et al*., 2012). Of interest would be if the
435 removal of the TM anchor (*Zm*SPI1) or addition of such anchor to *Zm*YUC1 would
436 change these phenotypes or the capacity of auxin production.

Possible benefits to the plant could be an additional level of regulation by subcellular compartmentation between cytosol and ER. The ER anchoring of auxin biosynthetic enzymes would bring them in close proximity to the transporters and signal proteins and maybe even conjugating or deconjugating enzymes to swop between active and active auxin molecules adding an additional level of regulation.

Especially in the maize system with two enzymes in consecutive steps (*Zm*TAR1 and *Zm*SPI1) of auxin biosynthesis anchored to the ER membrane, it might allow the enzymes to work in close proximity or even form metabolons hereby allowing metabolic channelling and enhancing productivity.

Experimental procedures

Cloning of expression plasmids

Primers were obtained from MWG Biotech. Q5 high-fidelity DNA polymerase (New England Biolabs) was used for all polymerase chain reaction reactions. Genes of interest were cloned into the modified binary vector PB7YWG2 containing a C-terminal YFP (Karimi *et al*., 2005). Vectors containing for maize genes *ZmYUC1* and *ZmTAR1* were kindly provided by Professor Prem Chourey; full-length *Zm*SPI1 and the N-termini of *ZmT*AR3 (aa 1-155) and *Zm*Vt2 (aa 1-140) were synthesised by MWG Biotech with codon optimisation.

Plant material and transient expression in tobacco leaves

For Agrobacterium-mediated transient expression, 5-week-old tobacco (*Nicotiana tabacum* SR1 cv Petit Havana) plants grown in the greenhouse were used. Transient expression was induced and detected according to Sparkes *et al*. (2006). In brief, each expression vector was introduced into Agrobacterium strain GV3101 by heat shock. A single colony from the transformants was inoculated into 5 ml of YEB medium (per litre: 5 g of beef extract, 1 g of yeast extract, 5 g of sucrose and 0.5 g of $MgSO_4 \cdot 7H_2O$) supplemented with 50 μg/ml spectinomycin and rifampicin. After overnight shaking at 25°C, 1 ml of the bacterial culture was pelleted by centrifugation at 2,200 × g for 5 min at room temperature. The pellet was washed twice with 1 ml of infiltration medium (50 mM MES, 2 mM $Na_3PO4 \cdot 12H_2O$, 0.1 mM acetosyringone and 5 mg/ml glucose) and then resuspended in 1 ml of infiltration buffer. The bacterial suspension was diluted to a final OD_{600} of 0.1 and gently pressed through the stomata on the lower epidermal surface using a 1 ml syringe. Transformed plants then were incubated under normal growth conditions for 48 h. Images were taken using a Zeiss LSM510 Meta laser scanning confocal microscope with 40x or 63x oil immersion objectives. For imaging of

GFP/YFP combinations, samples were excited using 458 and 514 nm laser lines in multi-track mode with line switching. Images were edited using the LSM510 image browser. For ratiometric imaging plant infiltration was performed as described above and ratiometric imaging of roGFP2 was performed as described by Wang *et al*. (2011). Data was analysed using the program Batch Ratio Analysis V1.3 (Dr M. Fricker, Oxford University; Schwarzländer *et al*., 2008)

ER microsome preparation

All steps were performed on ice or 4^{o}C unless indicated otherwise. Coleoptile (5 g) or primary root tissue (4 days after germination) were ground in liquid nitrogen using a mortar and pestle and homogenised in approximately 4 ml of buffer A (25 mM TEA-HOAc pH7.5, 50 mM KOAc pH7.5, 5 mM $Mg(OAc)_2$, 0.25 M sucrose, 4 mM DTT). 4 ml of buffer B (100 mM TEA-HOAc pH7.5, 20 mM EDTA) was added and the suspension was incubated on ice for 10 min. Afterwards the homogenate was spun at 1,000 g for 10 min. The resulting supernatant was poured over cheese cloth into a fresh tube. That extract was spun again at 4,500 g for 25 min. In ultracentrifuge tubes the 8 ml suspension were layered on 4 ml of sucrose cushion (buffer C: 25 mM TEA-HOAc pH7.5, 25 mM KOAc pH7.5, 2 mM $Mg(OAc)_2$, 0.5 M sucrose, 4 mM DTT). This was spun for 90 min at 93,000 g (swing-out rotor; SW41) for 90 min. The final pellet was resuspended in 200 µl buffer D (25 mM TEA-HOAc pH7.5, 0.25M sucrose, 1 mM DTT) using a glass rod and a 2 ml Potter-Elvehjem homogeniser. Freshly prepared microsomes were used for enzymatic assays.

IAA quantification

Enzymatic activity tests with microsomal and cytosolic fractions were carried out in 100 mM Tris-HCl, pH 8.0, using 20 µl plant extract, 1 mM NADPH, 100 µM FAD and 100

499 µM Trp or IPA in a total volume of 100 µl. After incubation for 1 h in a 37ºC water bath
500 the assays were snap-frozen in liquid nitrogen and IAA extracted by ethyl acetate
501 phase separation (Park *et al*., 2003; Kriechbaumer *et al*., 2007). In brief: The pH of the
502 sample was adjusted higher than 9.5 with 1 M Na_2CO_3, and the sample was then
503 extracted with 400 µl ethyl acetate. The aqueous lower phase was recovered, 200 µl
504 water were added and the partitioning procedure was repeated and again the aqueous
505 phase was recovered and combined with the aqueous phase from the first partitioning
506 step. The collected aqueous phase was acidified with acetic acid to a pH below 2.5 and
507 partitioned twice with addition of 400 µl ethyl acetate for each step. The organic phases
508 were collected and the liquid evaporated using a speed-vac (Centrivap, Labconco).
509 The dried substances were re-dissolved in 100% methanol and analysed via HPLC
510 with a reverse-phase column (Apollo C18, 250 mm x 4.6 mm, 5 µm, Grace). IAA was
511 quantified via a HPLC system (Waters 600E) in isocratic flow of 0.8 ml/min with a 40:60
512 mixture of buffer A (10% methanol, 0.3% acetate) and buffer B (90% methanol, 0.3%
513 acetate). Peaks were identified by comparison with the standard substances with
514 respect to retention time and UV spectrum using both a UV monitor (Waters 486) as
515 well as a fluorescence monitor (Waters 470).
516
517 IAA produced in tobacco leaves after infiltration with *Zm*SPI1-YFP, *Zm*TAR1-YFP and
518 *Zm*YUC1-YFP constructs was isolated and quantified as described above
519
520 **Quantification of IAA by GC-MS**
521 IAA produced in the reactions was purified by HPLC as described above. 2,4,5,6,7-
522 pentadeuteriated IAA (Cambridge Isotope Laboratories, UK) was included as internal
523 standard. HPLC fractions collected in Eppendorf tubes were completely dried under
524 vacuum and dissolved in 20 µl of methanol. Then 50 µl ethereal diazomethane (Sigma-
525 Aldrich) was added to each sample for derivatization. The mixture was kept at room

526 temperature for 30 min in a fume hood. Three pin holes were made on the top of each
527 Eppendorf tube and the tubes were set to dry in a speed-vac (Centrivap, Labconco) for
528 10 min. The remaining solution in the Eppendorf tubes was blown off with a gentle
529 stream of pure N_2 gas. The derivatized samples were dissolved in 5 or 10 µl of pure
530 methanol and 1 µl of the solution was injected to GC-MS (CP-3800, Saturn 2200,
531 Varian) in the split-less mode. The identity of derivatized IAA was confirmed by 130 and
532 189 fragmentation ions and normalized against the internal standard recognized by 135
533 and 184 fragmentation ions. The signals obtained in the quantification were all in the
534 linear range that was established with external standards. The peak area of 130
535 fragmentation ion was integrated and used for the determination of the amount of IAA
536 produced.
537
538 **Western blotting of microsomal and cytosolic fraction**
539 100 µg of total protein extract, the cytosolic and microsomal fractions, respectively,
540 were separated on a 12% (v/v) SDS-PAGE gel, transferred to a nitrocellulose
541 membrane, and probed with maize nitrilase-specific antibodies (1:400), anti-H+ATPase
542 antibodies (1:1000, Agrisera) or anti-AOX1/2 antibodies (1:1000, Agrisera),
543 respectively. The membrane was further incubated with anti-rabbit immunoglobulin G
544 conjugated with Cy5, and the signal was detected with a fluorescence scanner using a
545 red fluorescence filter.
546
547 **Supplementary material:**
548 Supplementary Figure 1: GC-MS chromatogram traces for IAA.
549 Supplementary Figure 2A: Comparison of GC-MS and HPLC analysis for enzymatic
550 conversion of Trp and IPA to IAA.
551 Supplementary Figure 2B: Ratios of auxin activity in microsomal and cytosolic fractions
552 compared in GC-MS and HPLC data.

Acknowledgements

The authors thank Prof Prem Chourey (University of Florida) for kindly supplying *ZmTAR1* and *ZmSPI1* plasmids. We thank Chanwoo Park, Minjae Kim, Jongyoon Ho and Simon Giles for their kind help and technical support and Dr Mark Fricker (Oxford University) for the Batch Ratio Analysis V1.3 program.

V.K. was supported by a BBSRC research grant awarded to C.H. and a research scholarship from Korean Federation of Science and Technology Societies (KOFST) awarded to V.K.

References

Abell BM, Holbrook LA, Abenes M, Murphy DJ, Hills MJ, Moloney MM. 1997. Role of the proline knot motif in oleosin endoplasmic reticulum topology and oil body targeting. Plant Cell **9**, 1481–1493.

Bandurski RS.1980. Homeostatic control of concentrations of indole-3-acetic acid. Plant Growth Substances 1979 (Skoog,F.,ed.) 37–49,Springer-Verlag, Berlin and Heidelberg.

Barbez E, Kubes M, Rolcik J, Beziat C, Pencik A, Wang B, Rosquete MR, Zhu J, Dobrev PI, Lee Y, Zažímalovà E, Petrášek J, Geisler M, Friml J, Kleine-Vehn J. 2012. A novel putative auxin carrier family regulates intracellular auxin homeostasis in plants. Nature **485**, 119–122.

Barbez E, Kleine-Vehn J. 2013. Divide Et Impera--cellular auxin compartmentalization. Current Opinion in Plant Biology **16**, 78–84.

Bernardi J, Lanubile A, Li Q-B, Kumar D, Kladnik A, Cook SD, Ross JJ, Marocco A, Chourey PS. 2012. Impaired auxin biosynthesis in the defective endosperm18 mutant is due to mutational loss of expression in the ZmYuc1 gene encoding endosperm-specific YUCCA1 protein in maize. Plant Physiology **160**, 1318–1328.

Bernsel A, Viklund H, Hennerdal A, Elofsson A. 2009. TOPCONS: consensus prediction of membrane protein topology. Nucleic Acids Research **37**, W465–8.

Bitto E, Bingman CA, Bittova L, Houston NL, Boston RS, Fox BG, Phillips GN Jr. 2009. X-ray structure of ILL2, an auxin-conjugate amidohydrolase from Arabidopsis thaliana. Proteins **74**, 61–71.

Brach T, Soyk S, Muller C, Hinz G, Hell R, Brandizzi F, Meyer AJ. 2009. Non-invasive topology analysis of membrane proteins in the secretory pathway. Plant Journal **57**, 534–541.

Cheng Y, Dai X, Zhao Y. 2006. Auxin biosynthesis by the YUCCA flavin monooxygenases controls the formation of floral organs and vascular tissues in Arabidopsis. Genes Dev **20**, 1790–1799.

Chourey PS, Li QB, Kumar D. 2010. Sugar-hormone cross-talk in seed development: two redundant pathways of IAA biosynthesis are regulated differentially in the invertase-deficient miniature1 mn1) seed mutant in maize. Molecular Plant **3**, 1026–1036.

Chuong SDX, Good AG, Taylor GJ, Freeman MC, Moorhead GBG, Muench DG. 2004. Large-scale identification of tubulin-binding proteins provides insight on

subcellular trafficking, metabolic channelling and signalling in plant cells. Molecular Cell Proteomics **3**, 970–983.

Dai X, Mashiguchi K, Chen Q, Kasahara H, Kamiya Y, Ojha S, DuBois J, Ballou D, Zhao Y. 2013. The biochemical mechanism of auxin biosynthesis by an arabidopsis YUCCA flavin-containing monooxygenase. J Biol Chem **18**, 1448–1457.

Dal Bosco CD, Dovzhenko A, Liu X, Woerner N, Rensch T, Eismann M, Eimer S, Hegermann J, Paponov IA, Ruperti B, Heberle-Bors E, Touraev A, Cohen JD, Palme K. 2012. The endoplasmic reticulum localized PIN8 is a pollen-specific auxin carrier involved in intracellular auxin homeostasis. Plant Journal **71**, 860–870.

Darwin C, Darwin F. 1880. The power of movement in plants. London: John Murray.

Friml J, Jones AR. 2010. Endoplasmic reticulum: the rising compartment in auxin biology. Plant Physiology **154**, 458–462.

Gallavotti A, Barazesh S, Malcomber S, Hall D, Jackson D, Schmidt RJ, McSteen P. 2008. sparse inflorescence1 encodes a monocot-specificYUCCA-like gene required for vegetative and reproductive development in maize. PNAS **39**, 15196–15201.

Grefen C, Stadele K, Ruzicka K, Obrdlik P, Harter K, Horak J. 2008. Subcellular localization and in vivo interactions of the Arabidopsis thaliana ethylene receptor family members. Mol Plant **1**, 308–320.

Hrazdina G, Wagner GJ. 1985. Metabolic pathways as enzyme complexes: Evidence for the synthesis of phenylpropanoids and flavonoids on membrane associated enzyme complexes. Archives of Biochemistry and Biophysics **237**, 88–100.

Jarvis P, Chen LJ, Li H, Peto CA, Fankhauser C, Chory J. 1998. An Arabidopsis mutant defective in the plastid general protein import apparatus. Science **28**, 100–103.

Jørgensen K, Rasmussen AV, Morant M, Nielsen AH, Bjarnholt N, Zagrobelny M, Bak S, Møller BL. 2005. Metabolon formation and metabolic channeling in the biosynthesis of plant natural products. Current Opinion in Plant Biology **8**, 280–291.

Karimi M, De Meyer B, Hilson P. 2005. Molecular cloning and expression of tagged fluorescent protein in plant cells. Trends in Plant Science **10**, 103–105.

Kim JI, Sharkhuu A, Jin JB, Li P, Jeong JC, Baek D, Lee SY, Blakeslee JJ, Murphy AS, Bohnert HJ, Hasegawa PM, Yun DJ, Bressan RA. 2007. yucca6, a dominant mutation in Arabidopsis, affects auxin accumulation and auxin-related phenotypes. Plant Physiology **145**, 722–735.

Kögl F, Haagen-Smit AJ, Erxleben H. 1934. Über ein neues Auxin (Heteroauxin) aus Harn. 11. Mitteilung über pflanzliche Wachstumsstoffe. Z Physiol Chemie **228**, 90–103.

Koga J, Adachi T, Hidaka H. 1992. Purification and characterization of indolepyruvate decarboxylase: a novel enzyme for indole-3-acetic acid biosynthesis in Enterobacter cloacae. Journal of Biological Chemistry **267**, 15823–15828.

Kriechbaumer V, Park WJ, Piotrowski M, Meeley RB, Gierl A , Glawischnig E. 2007. Maize nitrilases have a dual role in auxin homeostasis and beta-cyanoalanine hydrolysis. Journal of Experimental Botany **58**, 4225–4233.

Kriechbaumer V, Wang P, Hawes C, Abell BM. 2012. Alternative splicing of the auxin biosynthesis gene YUCCA4 determines its subcellular compartmentation. Plant Journal **70**(2), 292-302.

Labarca C, Nicholls PB, Bandurski RS. 1965. A partial characterization of indoleacetylinositols from ZEA mays. Biochem Biophys Res Commun **20**(5), 641**–**646.

LeClere S, Schmelz EA, Chourey PS. 2010. Sugar levels regulate tryptophan-dependent auxin biosynthesis in developing maize kernels. Plant Physiology **153**, 306–318.

Ludwig-Müller J, Decker EL, Reski R. 2009. Dead end for auxin conjugates in Physcomitrella? Plant Signaling & Behavior **4**, 116–118.

Ludwig-Müller J, Julke S, Bierfreund NM, Decker EL, Reski R. 2009. Moss Physcomitrella patens) GH3 proteins act in auxin homeostasis. New Phytologist **181**, 323–338.

Ludwig-Müller J. 2011. Auxin conjugates: their role in plant development and in the evolution of land plants. Journal of Experimental Botany **62**, 1757–1773.

Martinière A, Lavagi I, Nageswaran G, Rolfe DJ, Maneta-Peyret L, Luu DT, Botchway SW, Webb SE, Mongrand S, Maurel C, Martin-Fernandez ML, Kleine-Vehn J, Friml J, Moreau P Runions J. 2012. Cell wall constrains lateral diffusion of plant plasma-membrane proteins. PNAS **109**, 12805–12810.

Mashiguchi K, Tanaka K, Sakai T, Sugawara S, Kawaide H, Natsume M, Hanada A, Yaeno T, Shirasu K, Yao H, McSteen P, Zhao Y, Hayashi K, Kamiya Y, Kasahara H. 2011. The main auxin biosynthesis pathway in Arabidopsis. PNAS **108**, 18512–18517.

Møller BL. 2010. Dynamic metabolons. Science **330**(6009), 1328–1329.

Mravec J, Skupa P, Bailly A, Hoyerova K, Krecek P, Bielach A, Petrasek J, Zhang J, Gaykova V, Stierhof YD, Dobrev PI, Schwarzerová K, Rolcík J, Seifertová D, Luschnig C, Benková E, Zazímalová E, Geisler M, Friml J. 2009. Subcellular homeostasis of phytohormone auxin is mediated by the ER localized PIN5 transporter. Nature **459**, 1136–1140.

Normanly J, Bartel B. 1999. Redundancy as a way of life – IAA metabolism. Current Opinion in Plant Biology **2**, 207–213.

Östin A, Ilic N, Cohen JD. 1999. An in vitro system from maize seedlings for tryptophan-independent indole-3-acetic acid biosynthesis. Plant Physiology **119**, 173–178.

Park WJ, Kriechbaumer V, Müller A, Piotrowski M, Meeley RB, Gierl A, Glawischnig E. 2003. The nitrilase ZmNIT2 converts indole-3-acetonitrile to indole-3-acetic acid. Plant Physiology **133**, 794–802.

Phillips KA, Skirpan AL, Liu X, Christensen A, Slewinski TL, Hudson C, Barazesh S, Cohen JD, Malcomber S, McSteen P. 2011. vanishing tassel2 encodes a grass-specific tryptophan aminotransferase required for vegetative and reproductive development in maize. The Plant Cell **23**, 550–566.

Rampey RA, LeClere S, Kowalczyk M, Ljung K, Sandberg G, Bartel B. 2004. A family of auxin-conjugate hydrolases that contributes to free indole-3-acetic acid levels during Arabidopsis germination. Plant Physiology **135**(2), 978–988.

Schwarzländer M, Fricker MD, Müller C, Marty L, Brach T, Novak J, Sweetlove LJ, Hell R, Meyer AJ. 2008. Confocal imaging of glutathione redox potential in living plant cells. Journal of Microscopy **231**(2), 299–316.

Sparkes IA, Runions J, Kearns A, Hawes C. 2006. Rapid, transient expression of fluorescent fusion proteins in tobacco plants and generation of stably transformed plants. Nature Protocols **1**, 2019–2025.

Stepanova AN, Robertson-Hoyt J, Yun J, Benavente LM, Xie DY, Dolezal K, Schlereth A, Jürgens G, Alonso JM. 2008. TAA1-mediated auxin biosynthesis is essential for hormone crosstalk and plant development. Cell **11**, 177–191.

Stepanova AN, Yun J, Robles LM, Novak O, He W, Guo H, Ljung K, Alonso JM. 2011. The Arabidopsis YUCCA1 flavin monooxygenase functions in the indole-3-pyruvic acid branch of auxin biosynthesis. The Plant Cell **23**, 3961–3973.

Tao Y, Ferrer JL, Ljung K, Pojer F, Hong FX, Long JA, Li L, Moreno JE, Bowman ME, Ivans LJ, Cheng Y, Lim J, Zhao Y, Ballaré CL, Sandberg G, Noel JP, Chory J. 2008. Rapid synthesis of auxin via a new tryptophan-dependent pathway is required for shade avoidance in plants. Cell **133**, 164–176.

Stafford HA. 1974. Possible multienzyme complexes regulating the formation of C6-C3 phenolic compounds and lignins in higher plants. Recent Advances in Phytochemistry **8**, 53–79.

Szerszen JB, Szczyglowski K, Bandurski RS. 1994. iaglu, a gene from Zea mays involved in conjugation of growth hormone indole-3-acetic acid. Science **265**(5179), 1699–1701.

Tivendale ND, Ross JJ, Cohen JD. 2014. The shifting paradigm of auxin biosynthesis. Trends in Plant Science **19**, 44–51.

Ueda M, Bandurski RS. 1974. Structure of indole-3-acetic Acid myoinositol esters and pentamethyl-myo-inositols. Phytochemistry **13**, 243–253

Van den Berg B, Clemons WM, Collinson I, Modis Y, Hartmann E, Harrison SC, Rapoport TA. 2004. X-ray structure of a protein conducting channel. Nature **427**, 36–44.

Wabnik K, Kleine-Vehne J, Govaerts W, Friml J. 2011. Prototype cellto- cell auxin transport mechanism by intracellular auxin compartmentalization. Trends in Plant Science **16**, 468–475.

Wang P, Hummel E, Osterrieder A, Meyer AJ, Frigerio L, Sparkes I, Hawes C. 2011. KMS1 and KMS2, two plant endoplasmic reticulum proteins involved in the early secretory pathway. Plant Journal **66**, 613–628.

Werhahn W, Niemeyer A, Jansch L, Kruft V, Schmitz UK, Braun H. 2001. Purification and characterization of the preprotein translocase of the outer mitochondrial membrane from Arabidopsis. Identification of multiple forms of TOM20. Plant Physiology **125**, 943–954.

Winkel BSJ. 2004. Metabolic channeling in plants. Annual Review of Plant Biology **55**, 85–107.

Winkel-Shirley B. 2001. Flavonoid biosynthesis: a colorful model for genetics, biochemistry, cell biology and biotechnology. Plant Physiology **126**, 485–493.

Woodward AW, Bartel B. 2005. Auxin: regulation, action, and interaction. Annals of Botany **95**, 707–735.

Zajchowski LD, Robbins SM. 2002. Lipid rafts and little caves. European Journal of Biochemistry **269**, 737–752.

Tables:

Table 1: *In silico* prediction of transmembrane domains (TMD) with the computational algorithms TMHMM and prediction of signal peptides (SP) with SignalP4.1 (http://www.expasy.org/tools/).

Protein	**TMHMM**	**SignalP4.1**
*Zm*SPI1	N-term TMD (aa 20-42)	No SP predicted.
*Zm*TAR1	N-term TMD (aa 13-35)	No SP predicted
*Zm*TAR3	N-term TMD (aa7-29)	Signal peptide, cleavage site between aa 24 / 25
*Zm*YUC1	no TMD predicted	No SP predicted
*Zm*VT2	no TMD predicted	No SP predicted

Figure legends:

Figure 1: Predicted transmembrane domains (TMD) in the amino acid sequence of auxin biosynthetic proteins catalysing the conversion of Trp to IPA (left: *Zm*TAR1, *Zm*TAR3 and *Zm*VT2) and the following enzymatic step from IPA to IAA (right: *Zm*SPI1 and *Zm*YUC1), respectively. Shown is a hydrophobicity plot using the prediction software TMHMM on the ExPASy server (http://www.expasy.org/tools/) with the potential TMD in red.

Figure 2: Immunoblot analysis of microsomal fractions.

A) Immunoblot analysis of nitrilase proteins in maize microsomal (M) and cytosolic (C) fraction. Western blots of 100 µg of protein from each fraction were probed with diluted (1:400) anti-*Zm*NIT1 antibodies recognizing both maize nitrilases.

B) Immunoblot analysis of plasma membrane H+ATPase proteins and mitochondrial alternative oxidases (AOX1/2) in maize total protein extract (T) and microsomal (M) fraction. Western blots of 100 µg of protein from each fraction were probed with diluted (1:1000) antibodies.

Figure 3: Enzymatic conversion of Trp (grey bars) and IPA (white bars) to IAA by microsomal (Micro) fractions, cytosolic (Cyt) fractions or total plant extract from A) maize coleoptiles (Col) and B) primary roots (PR) 4 days after germination. Standard errors and percentages normalised to total plant extract are indicated. n=2 (2 biological samples with 3 replica each.

Figure 4: Transient expression and localisation of auxin biosynthetic proteins in tobacco leaf cells.

Coexpression with the ER luminal marker GFP-HDEL is shown for *Zm*SPI1YFP (1), *Zm*TAR1 (2) and *Zm*YUC1 (3). *Zm*YUC1 was also coexpressed with the plasma membrane marker LTI6b (4). The N-termini containing the sequence of potential TMDs of *Zm*VT2 (5) and *Zm*TAR3 (6) were also compared to expression patterns of GFP-HDEL.

Figure 5: Ratiometric redox assays for roGFP2-tagged *Zm*SPI1 (lane 1) and *Zm*TAR1 (lane 2). The ratio of 405 and 488 nm excitation is determined by the redox state of roGFP2. In blue: cytosolic environment; in red: ER luminal environment. Cytosolic roGFP2 (lane 3) and the ER lumen marker roGFP2–HDEL (lane 4) were used as controls for ER and cytosol localisation, respectively. The mean 405 nm/488 nm ratio is indicated on the right for each construct.

Figure 6: Functional assays for tagged auxin biosynthetic enzymes.

A) Enzymatic conversion of IPA to IAA by protein extracts from tobacco leaves transiently expressing *Zm*SPI1 or *Zm*Vt2. Data is presented in % normalised to the control. Standard errors are indicated. n=3 (3 biological samples with 2 technical replica each). $*$ $p<0.05$.

B) Enzymatic conversion of Trp to IAA by protein extracts from tobacco leaves transiently expressing *Zm*TAR1. Data is presented in % normalised to the control. Standard errors are indicated. n=3 (3 biological samples with 2 technical replica each). $*$ $p<0.05$.

C) Total IAA content from tobacco leaves transiently expressing *Zm*SPI1, *Zm*TAR1 or *Zm*Vt2 compared to control plants expressing an empty vector. Data is presented in % normalised to the control. Standard errors are indicated. n=3 (3 biological samples with 2 technical replica each). $*$ $p<0.05$.

Figure 7: Dual compartmentation schematics for auxin function. Auxin biosynthesis (various TAR and YUCCA homologues localised to cytosol or ER), signalling (TIR1), conjugation (GH3, ILL), and transport (PIN, PILS) take place in cytosol and ER-linked.

YUCCA pathway in maize

Trp —TAR1/TAR3/VT2→ **IPA** —YUC1/SPI1→ **IAA**

Trp aminotransferase-related1 (*Zm*TAR1)

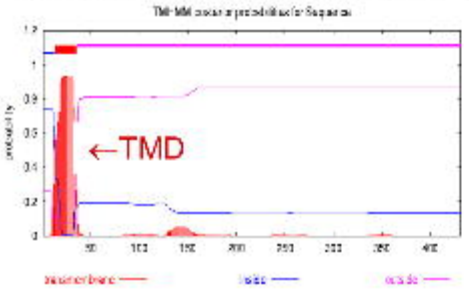

Sparse inflorescence1 (*Zm*SPI1)

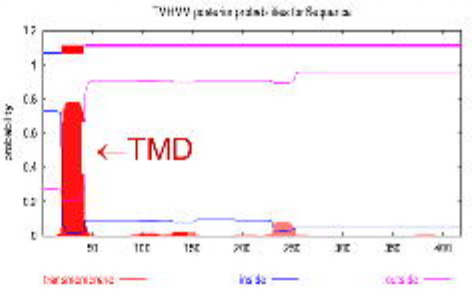

Trp aminotransferase-related3 (*Zm*TAR3)

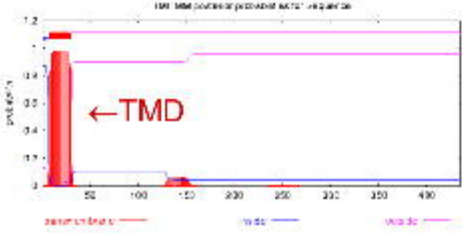

Vanishing tassel2 (*Zm*VT2)

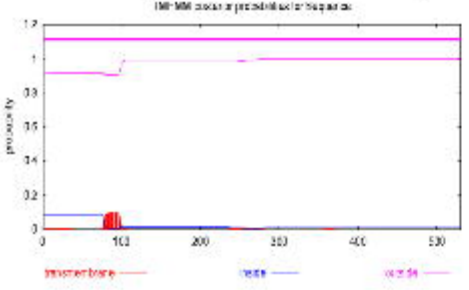

YUCCA1 (*Zm*YUC1)

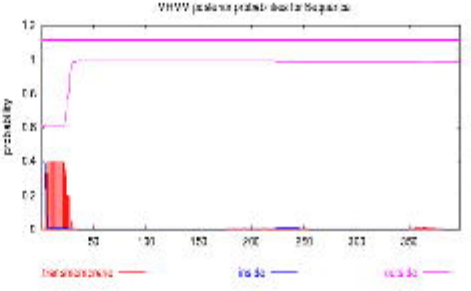

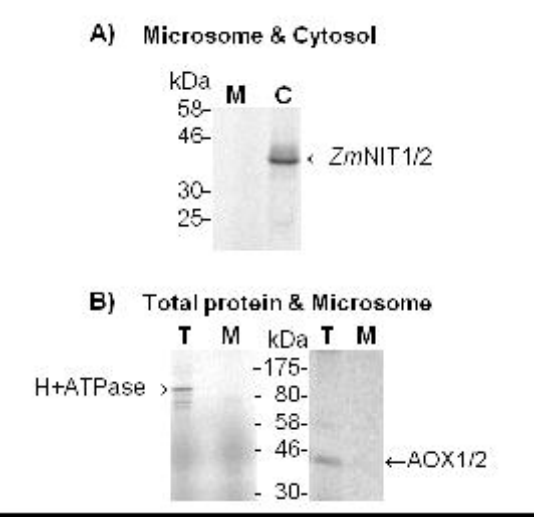
A) Microsome & Cytosol
kDa
M
C
58-
46-
30-
25-
ZmNIT1/2
B) Total protein & Microsome
T
M
kDa
T
M
H+ATPase
-175-
- 80-
- 58-
- 46-
- 30-
←AOX1/2

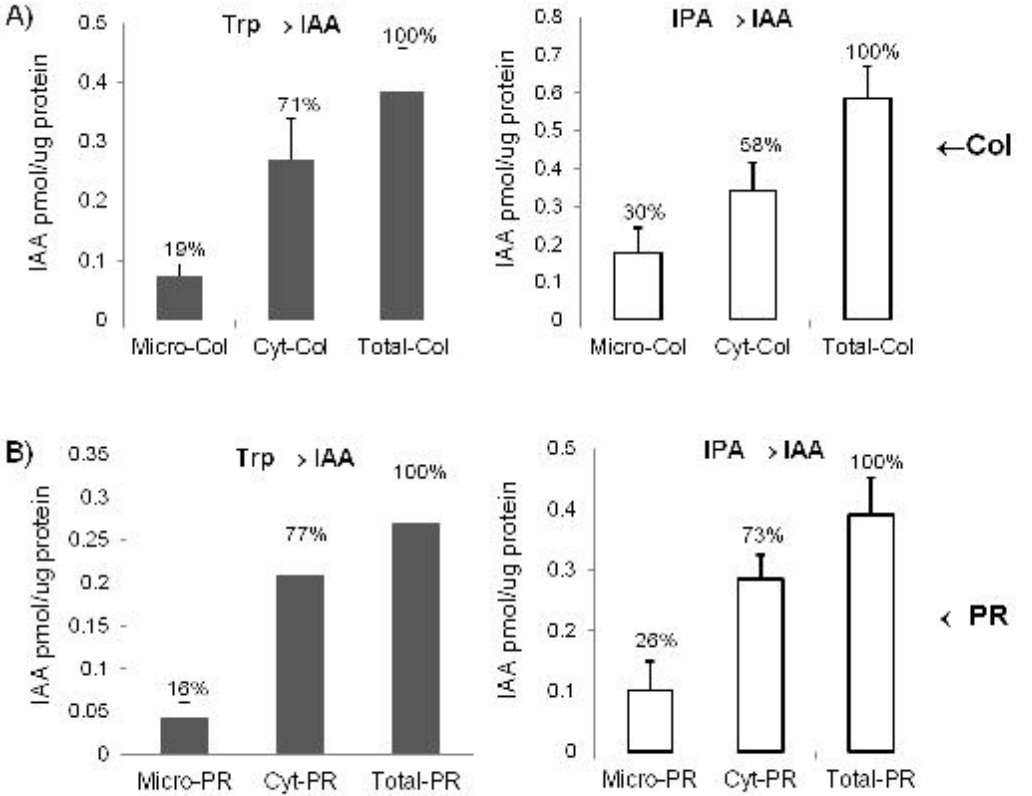
A)
Trp > IAA
IAA pmol/ug protein
0.5
0.4
0.3
0.2
0.1
0
19%
71%
100%
Micro-Col
Cyt-Col
Total-Col
IPA > IAA
IAA pmol/ug protein
0.8
0.7
0.6
0.5
0.4
0.3
0.2
0.1
0
30%
58%
100%
Micro-Col
Cyt-Col
Total-Col
←Col
B)
Trp > IAA
IAA pmol/ug protein
0.35
0.3
0.25
0.2
0.15
0.1
0.05
0
16%
77%
100%
Micro-PR
Cyt-PR
Total-PR
IPA > IAA
IAA pmol/ug protein
0.5
0.4
0.3
0.2
0.1
0
26%
73%
100%
Micro-PR
Cyt-PR
Total-PR
< PR

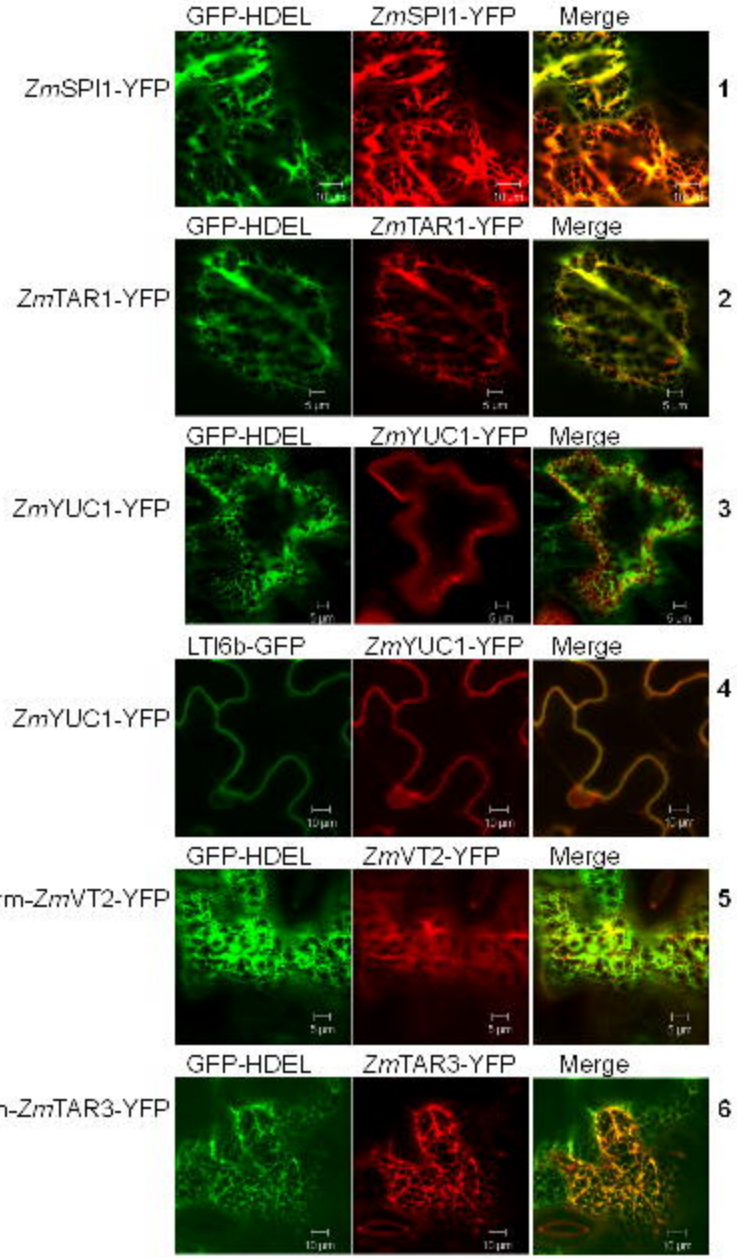
GFP-HDEL
ZmSPI1-YFP
Merge
ZmSPI1-YFP
1
GFP-HDEL
ZmTAR1-YFP
Merge
ZmTAR1-YFP
2
GFP-HDEL
ZmYUC1-YFP
Merge
ZmYUC1-YFP
3
LTI6b-GFP
ZmYUC1-YFP
Merge
ZmYUC1-YFP
4
GFP-HDEL
ZmVT2-YFP
Merge
N-term-ZmVT2-YFP
5
GFP-HDEL
ZmTAR3-YFP
Merge
N-term-ZmTAR3-YFP
6

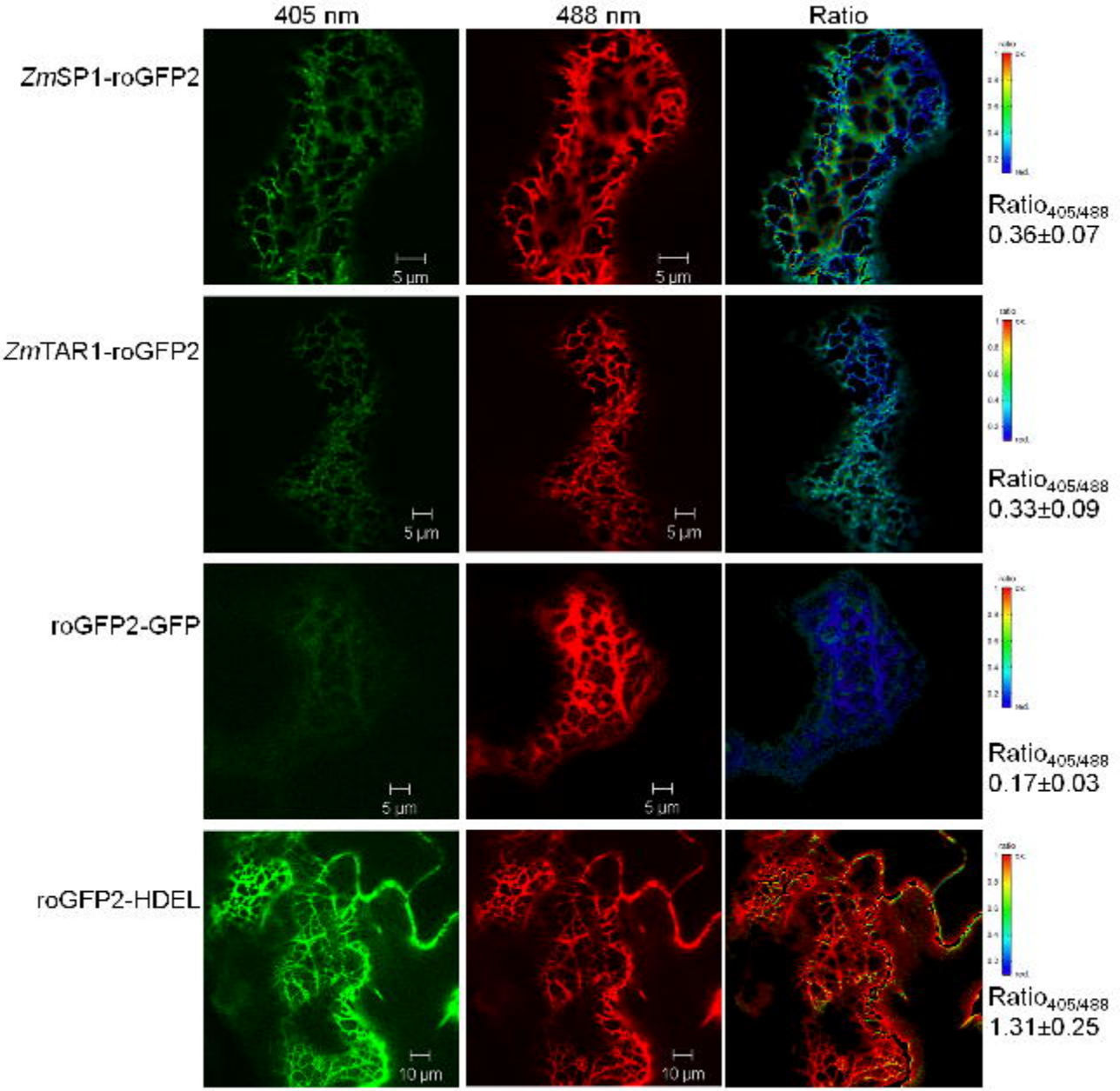
405 nm
488 nm
Ratio
ZmSP1-roGFP2
ZmTAR1-roGFP2
roGFP2-GFP
roGFP2-HDEL
5 µm
10 µm
Ratio405/488
0.36±0.07
Ratio405/488
0.33±0.09
Ratio405/488
0.17±0.03
Ratio405/488
1.31±0.25

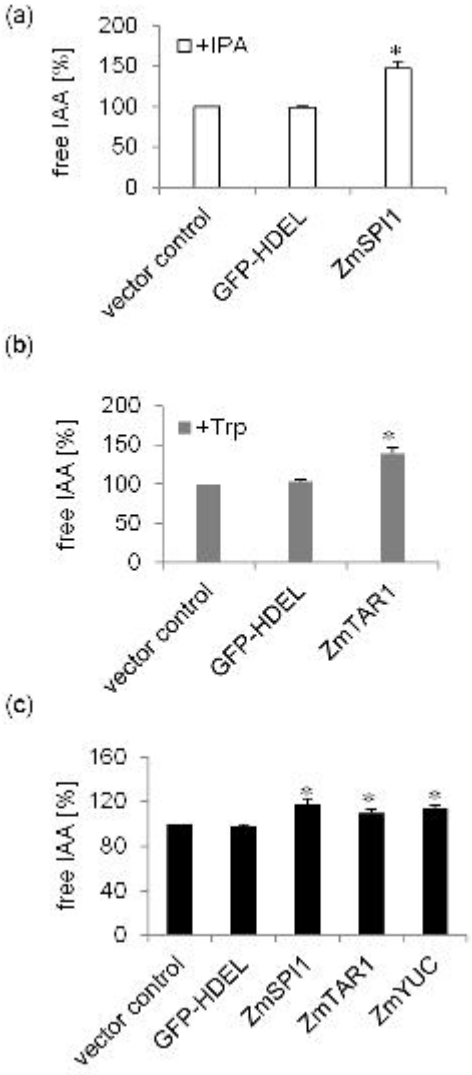
(a)
free IAA [%]
200
150
100
50
0
+IPA
*
vector control
GFP-HDEL
ZmSPI1
(b)
free IAA [%]
200
150
100
50
0
+Trp
*
vector control
GFP-HDEL
ZmTAR1
(c)
free IAA [%]
160
120
80
40
0
*
*
*
vector control
GFP-HDEL
ZmSPI1
ZmTAR1
ZmYUC

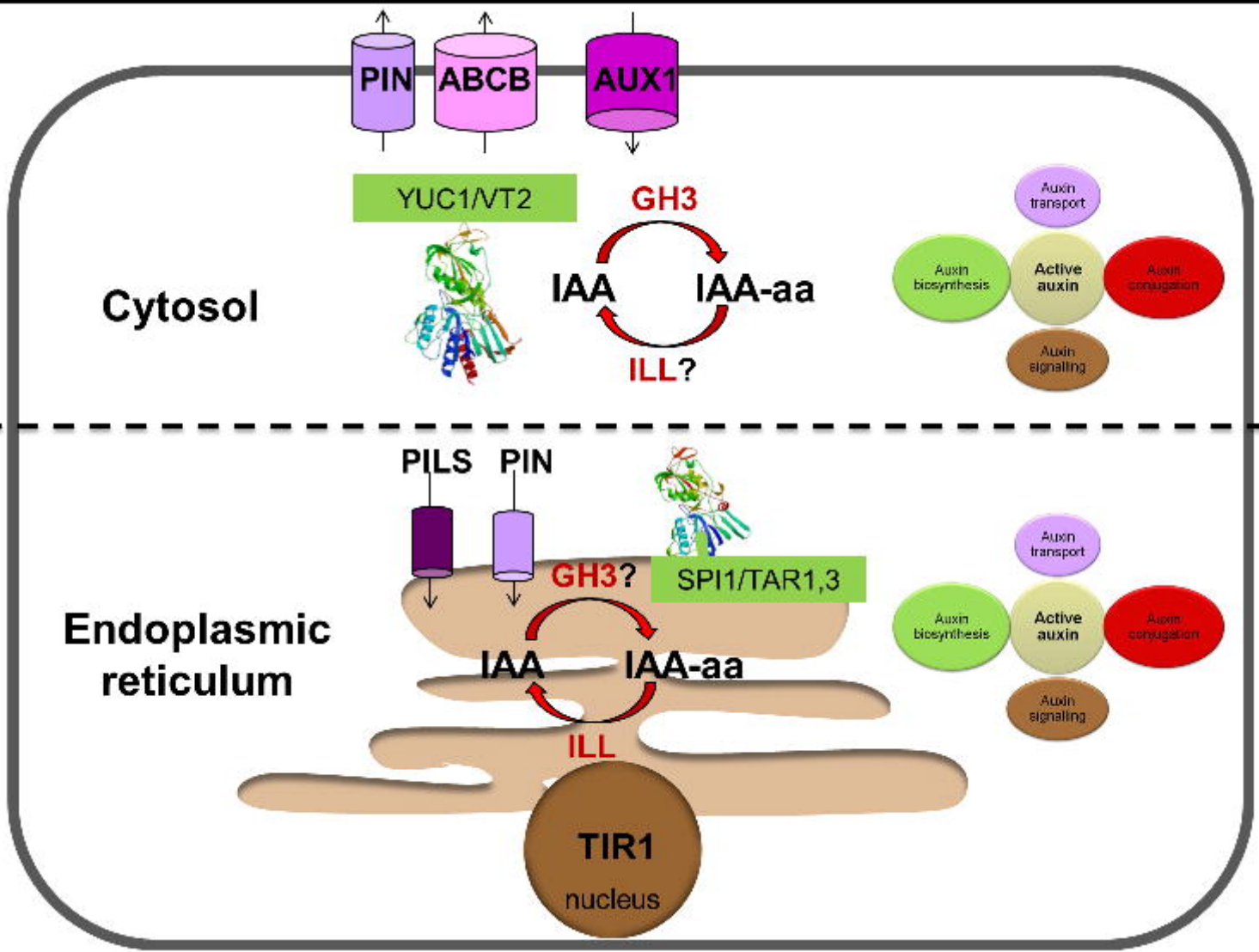
PIN
ABCB
AUX1
YUC1/VT2
GH3
IAA
IAA-aa
ILL?
Cytosol
Auxin transport
Auxin biosynthesis
Active auxin
Auxin conjugation
Auxin signaling
PILS
PIN
GH3?
SPI1/TAR1,3
IAA
IAA-aa
ILL
Endoplasmic reticulum
TIR1
nucleus

ER-localisation and activity of maize auxin biosynthetic enzymes

Verena Kriechbaumer, Hyesu Seo, Woong June Park, Chris Hawes

Supplementary Figure 1

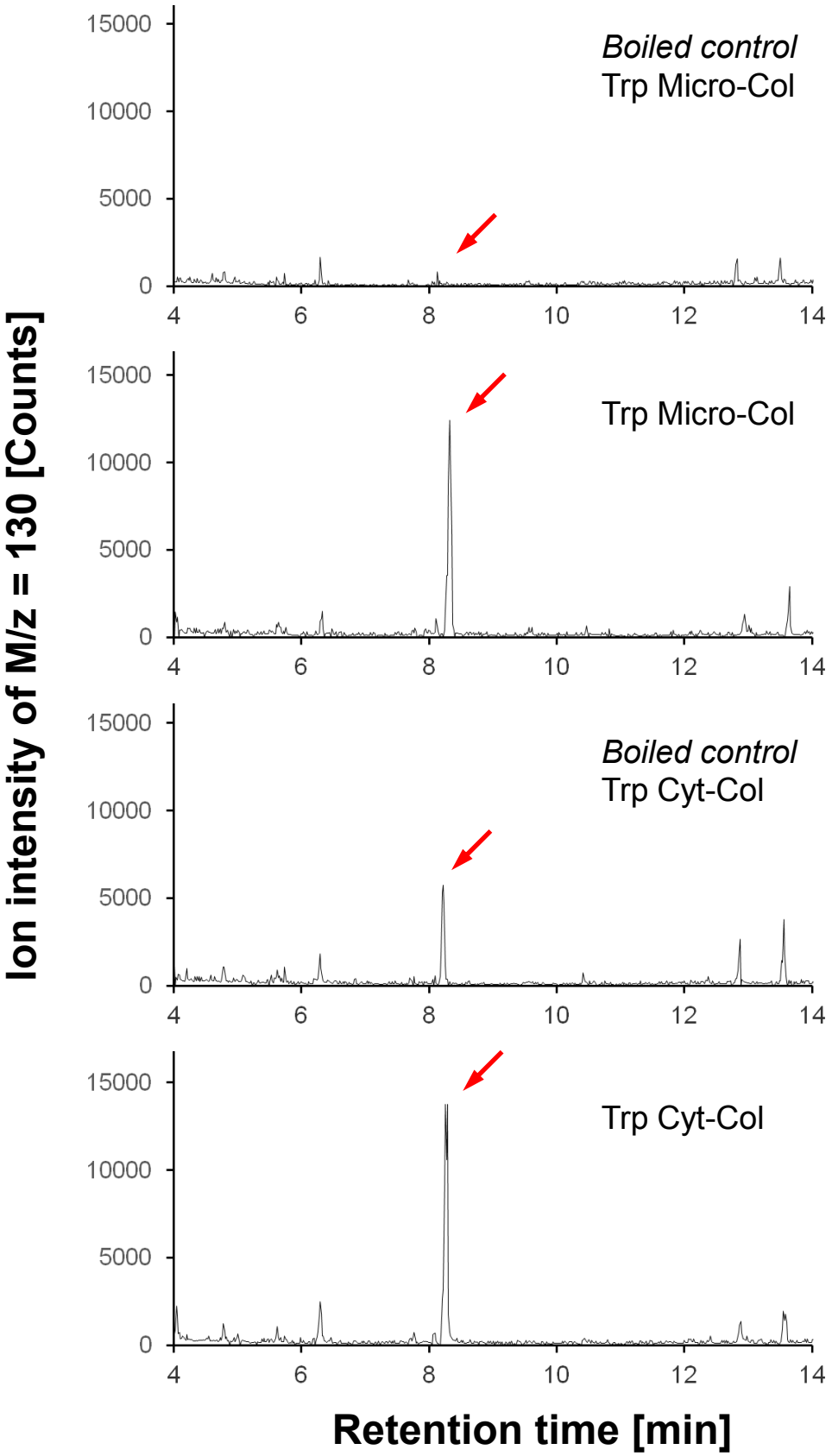

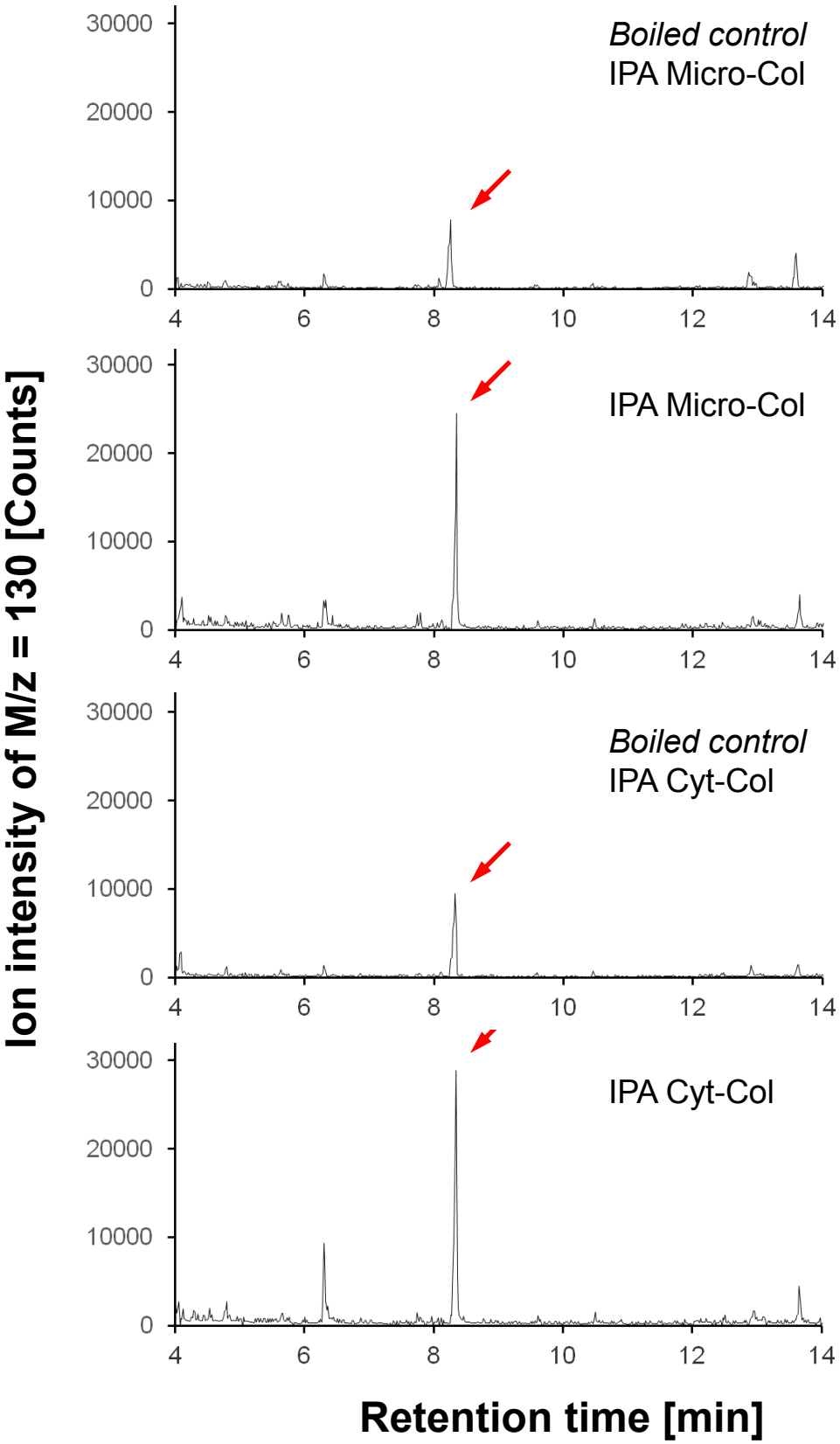

Supplementary Figure 1:
GC-MS chromatogram traces for IAA.
GC-MS traces for the conversion of Trp and IPA, respectively, to IAA by microsomal (Micro) fractions, cytosolic (Cyt) fractions from coleoptiles (Col). A boiled control for each conversion is included. The red arrow points out the IAA peak.

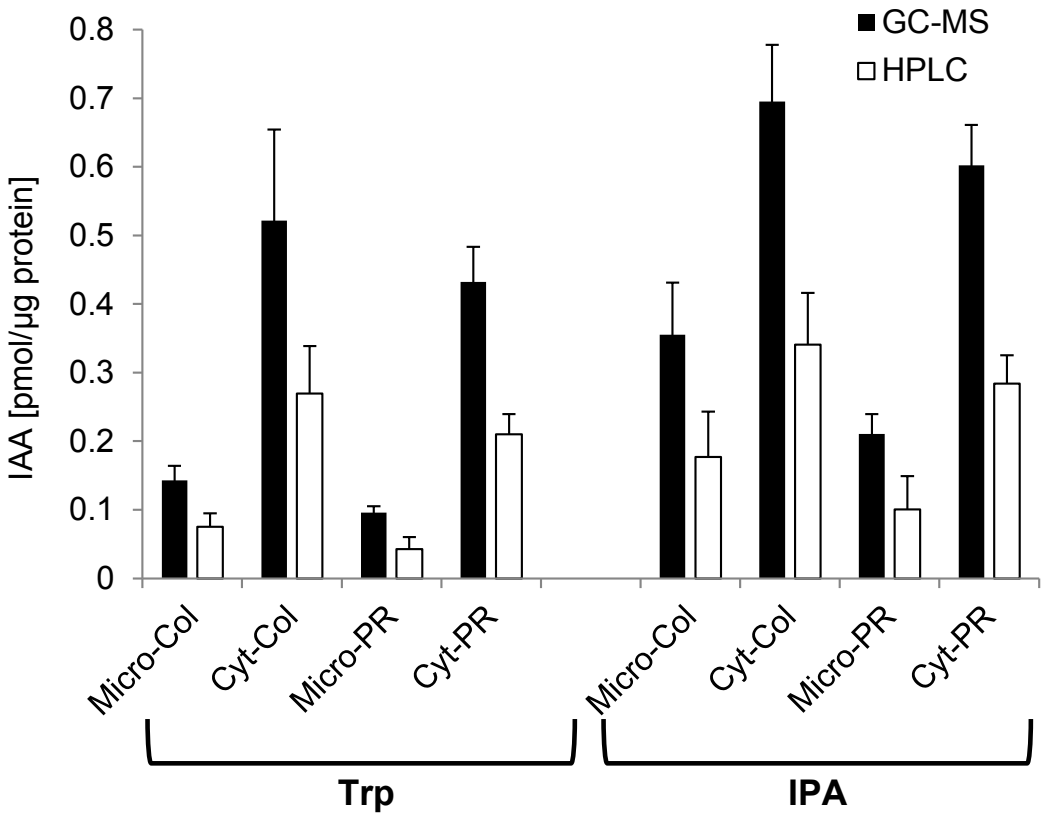

Supplementary Figure 2A:
Comparison of GC-MS and HPLC analysis.
Enzymatic conversion of Trp and IPA to IAA by microsomal (Micro) fractions, cytosolic (Cyt) fractions from coleoptiles (Col) or primary root (PR) tissue. The comparison of quantitative results using GC-MS (black bars) or HPLC with fluorescence detector (white bars) is shown. Standard errors are indicated. n=2 derived from at least two independent biological samples.

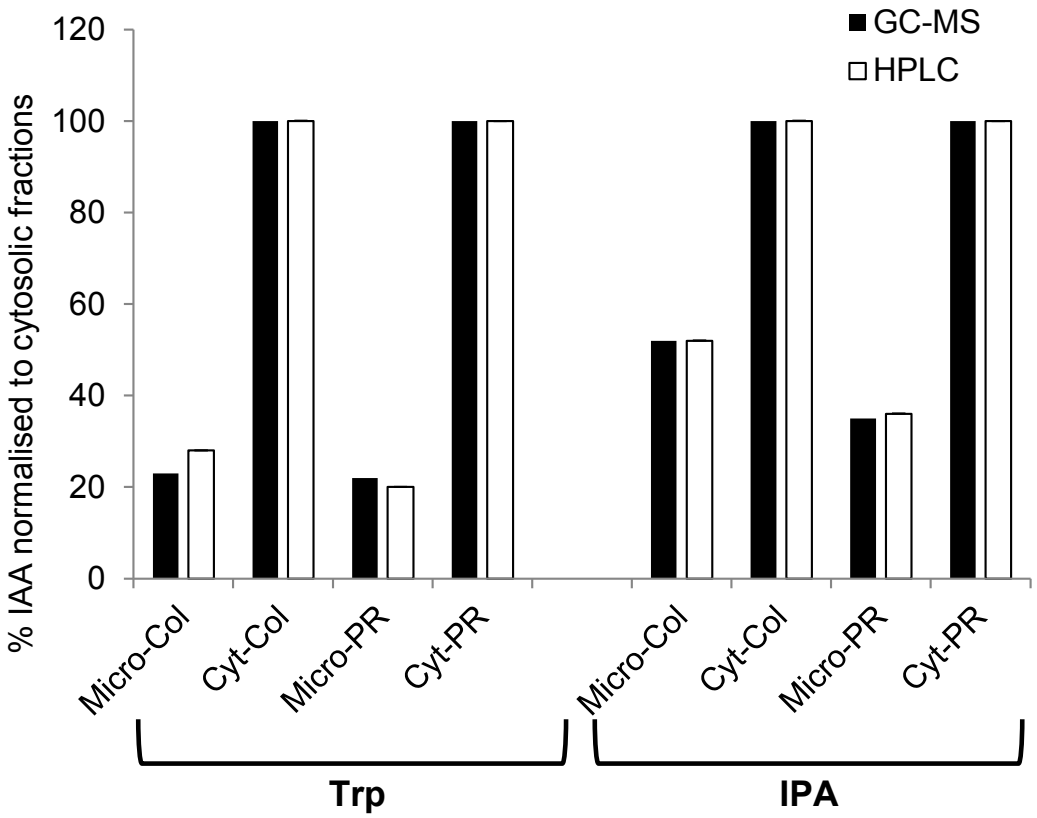

Supplementary Figure 2B:
Ratios of auxin activity in microsomal and cytosolic fractions compared in GC-MS (black bars) and HPLC (white bars) data. Data is presented in % normalised to the IAA production in the cytosolic fractions.